



Dielectric and energy-storage properties in $\text{Bi}_{0.5}\text{Na}_{0.5}\text{TiO}_3\text{-BaTiO}_3\text{-AgNbO}_3$ ternary perovskite compounds

Qi Xu¹ · Xuechen Huang² · Hanxing Liu³

Received: 8 March 2020 / Accepted: 13 May 2020 / Published online: 21 May 2020
© Springer Science+Business Media, LLC, part of Springer Nature 2020

Abstract

A ternary perovskite dielectric $(1-x)(0.92\text{Bi}_{0.5}\text{Na}_{0.5}\text{TiO}_3-0.08\text{BaTiO}_3)\text{-}x\text{AgNbO}_3$ has been developed for application as high-temperature energy-storage capacitors. It is suggested that with increasing AN content, the material has experienced non-ergodic relaxor \rightarrow ergodic relaxor \rightarrow paraelectric state transformation. The most attractive properties are obtained in the composition $x=0.10$ with superior high-temperature dielectric stability ($\epsilon_{r150^\circ\text{C}}=1901$, $\text{TCC}_{150^\circ\text{C}}\leq 15\%$ in 20–368 °C range) and optimized energy-storage performance ($W_{\text{max}}=1.07\text{ J/cm}^3$, $\eta_{\text{max}}=78\%$ at 10.4 kV/mm).

1 Introduction

Dielectric capacitors are widely used in pulsed power systems, electric vehicles, aerospace engineering, defense technology, and other fields [1]. The miniaturization, lightweight, and diversification of the design concepts in electronic components have raised higher requirements for the wide temperature stability and energy-storage performance of dielectric capacitors [2]. Therefore, in the development of new dielectric materials, wide temperature stability and high energy-storage density are equally important. It includes several aspects of the properties of dielectrics, including favorable dielectric properties and temperature stability, good electrical insulation, high energy-storage density, and energy-storage efficiency.

At present, dielectric materials with wide temperature stability and high energy-storage density are widely studied and reported. From the perspective of obtaining favorable dielectric temperature performance, $\text{BaTiO}_3\text{-Bi}(\text{Me}'\text{Me}'')\text{O}_3$ relaxors have been widely proposed. By forming solid

solution with layered $\text{Bi}(\text{Me}'\text{Me}'')\text{O}_3$, the sharp dielectric peak of BaTiO_3 can be depressed, which is in favor of stable $\epsilon_r\text{-}T$ curves. Such as in $0.8\text{BaTiO}_3\text{-}0.2\text{Bi}(\text{Mg}_{2/3}\text{Nb}_{1/3})\text{O}_3$ system, the working temperature range spanned from -50 to 125°C for $\pm 12\%$ tolerance with dielectric constant of ~ 700 and energy-storage density of 1.13 J/cm^3 [3]. On the other hand, from the perspective of obtaining superior energy-storage properties, linear dielectrics are the primary candidate due to the minimal energy loss. Lee [4] investigated $\text{Ca}(\text{Zr}, \text{Ti})\text{O}_3$ system and found that $\text{Ca}(\text{Zr}_{0.80}\text{Ti}_{0.20})\text{O}_3$ capacitors showed high electrostatic energy density of 4 J/cm^3 at 250°C in spite of low dielectric constant. In addition, glass is also regarded as a potential material with wide temperature stability and high energy-storage density. Although the permittivity of glass is relatively low, it has high breakdown strength, which is beneficial to high energy-storage density. But the dielectric properties of glass vary greatly with temperature, so the dielectric stability of glass needs further improvement by modification. Randall [5] has reported that alkali-free 12Ba-16B-9Al-63Si glass possessed stable permittivity of ~ 6.0 in the range of 20–180 °C with room temperature energy-storage density of 35 J/cm^3 .

In addition to the above three typical categories, $\text{Bi}_{0.5}\text{Na}_{0.5}\text{TiO}_3$ (BNT)-based system has drawn great attention in this field recently. It is commonly believed that BNT-based ceramics are relaxors instead of anti-ferroelectric material [6]. According to this theory, two phase structures (R3c and P4bm) co-exist as polar nanoregions over a wide temperature range and convert to each other as the temperature changes. Correspondingly, the dielectric and ferroelectric behavior has changed. The bimodal characteristics of the

✉ Qi Xu
xuqi17@cdu.edu.cn

¹ College of Materials and Chemistry & Chemical Engineering, Chengdu University of Technology, Chengdu 610059, China

² Department of Chemical and Materials Engineering, Chuzhou University, Chuzhou 239000, China

³ State Key Laboratory of Advanced Technology for Materials Synthesis and Processing, Wuhan University of Technology, Wuhan 430070, China

dielectric temperature spectrum of BNT-based solid solution are beneficial to the wide temperature stability, while the pinched hysteresis loop is beneficial to the high energy-storage density. BNT-based ceramics have shown a certain potential in the application of temperature stable capacitors and energy-storage capacitors, respectively [7–10]. However, there are few reports giving consideration to both high-temperature stability and energy-storage performance of this system. Besides, applying the relaxor theoretical model to specific BNT-based solid solution and combining structural changes and macroscopic properties remains to be explored.

In this paper, morphotropic phase boundary (MPB) composition $0.92\text{Bi}_{0.5}\text{Na}_{0.5}\text{TiO}_3\text{-}0.08\text{BaTiO}_3$ (BNT-BT) was selected as the matrix due to its more pinched P-E loop [11, 12]. Ag is a common element with the valence state of +1. As the electrode material of capacitors, a large number of researches focus on the influence of Ag electrode diffusion on the performance of the capacitors at present [13, 14], while relatively few researches directly introduce Ag into the system as one of the components. Therefore, we chose AgNbO_3 (AN) as the third member. A new ternary solid solution $(1-x)$ (BNT-BT)- x AN was synthesized. The phase structure, high-temperature dielectric properties, and energy-storage properties were systematically investigated.

2 Experimental procedure

2.1 Synthesis

Ceramic powders of $(1-x)$ (BNT-BT)- x AN ($x=0.01, 0.03, 0.05, 0.07, 0.10$) were prepared by high-temperature solid-state reaction method. Bi_2O_3 (purity 99.0%), Na_2CO_3 (purity 99.8%), TiO_2 (purity 98.5%), BaCO_3 (purity 99.0%), Nb_2O_5 (99.5%), and Ag_2O (purity 99.5%) were mixed stoichiometrically. The mixture was ball milled in alcohol solution for

24 h and dried. After the calcination at $800\text{ }^\circ\text{C}$ for 2 h, the powder mixtures were pressed into green pellets and sintered at temperatures between 1100 and $1120\text{ }^\circ\text{C}$ for 2 h. To minimize the evaporation of the volatile elements Bi and Na, the pellets were embedded in a powder of the same composition during sintering.

2.2 Characterization

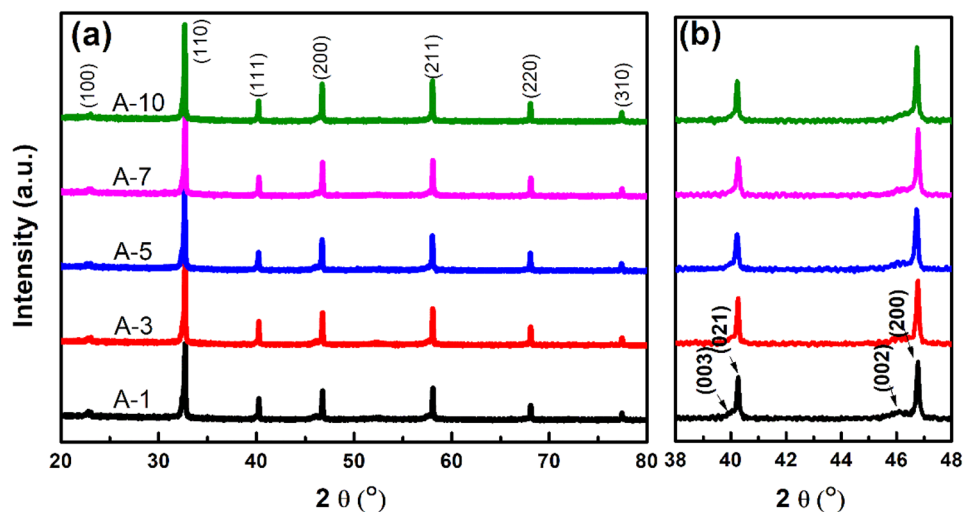
The crystal structure was examined using an X-ray powder diffractometer (PANalytical X'Pert PRO) with $\text{Cu K}\alpha$ radiation. The microstructure of the ceramics was taken by scanning electron microscope (Quanta 450 FEG, FEI) on the fresh cross-section. The average grain sizes were determined by the linear intercept method. The pellets were polished and coated with fire on silver paste at $500\text{ }^\circ\text{C}$ for 15 min as electrodes. Dielectric measurements were performed in a customer-designed furnace with a precision LCR meter (E4980A, Agilent) and a computer-controlled data collection system. The heating rate is $2\text{ }^\circ\text{C}/\text{min}$. RC time constant was calculated from the capacitance at 1 kHz and the DC resistance. P-E hysteresis loops and current curves were measured in a silicone oil bath using ferroelectric test system (HVI0403-239, Radiant Technology, USA). A triangular voltage waveform was selected for the electric field cycle.

3 Results and discussion

3.1 Structure characterization

Figure 1a shows the XRD patterns of $(1-x)$ (BNT-BT)- x AN ceramics with $2\theta=20\text{--}80^\circ$. All samples exhibited a single perovskite structure and no secondary phase was observed, which demonstrated that Ag^+ and Nb^{5+} were completely dissolved into the lattice of BNT-BT.

Fig. 1 **a** XRD patterns of $(1-x)$ (BNT-BT)- x AN ceramics. **b** Magnified view in the range from 38 to 48°



From the magnified view in the range $2\theta = 38\text{--}48^\circ$ in Fig. 1b, the sample $x = 0.01$ possessed split (003)/(021) and (002)/(200) peaks at $2\theta \approx 40^\circ$ and 46.5° , representing the coexistence of rhombohedral and tetragonal phases, respectively. With increasing AN content, the splitting peaks became increasingly symmetrical and gradually merged into single peak, respectively. For the composition $x = 0.10$, it became pseudo cubic structure.

Figure 2 shows the fresh cross-section SEM images of $(1 - x)$ (BNT-BT)- x AN ceramics sintered at optimum sintering temperature as listed in Table 1. All samples were thermally etched beforehand at 100°C lower than sintering temperature. Dense and homogeneous microstructure was obtained and all the compositions achieved relatively high densities (relative density $\rho > 97\%$). Besides, it can be detected that the grains became larger with the increase of AN content. The average grain size increased from $1.00\ \mu\text{m}$ in the composition $x = 0.01$ to $1.33\ \mu\text{m}$ in the composition $x = 0.10$, which was similar to that in BNT-BT-NN system [15]. It is known that grain growth in ceramics is related to mass transport. In the sintering process of BNT-BT-AN ceramics, vacancies would inevitably appear due to the volatilization of some A-site elements such as Na and Bi [15–17]. The appearance of vacancies, especially oxygen vacancies, provide favorable diffusion channel for particles, which is beneficial for mass transport. Thus, vacancies have been believed to be the main reason for grain growth in BNT-based ceramics [18].

Table 1 Composition, density, and grain size of $(1 - x)$ (BNT-BT)- x AN ceramic samples

Composition	Sample	Optimum sintering temperature ($^\circ\text{C}$)	Relative density (%)	Average grain size (μm)
$x = 0.01$	A-1	1120	97.5	1.00
$x = 0.03$	A-3	1120	97.9	1.03
$x = 0.05$	A-5	1120	97.6	1.11
$x = 0.07$	A-7	1120	97.7	1.25
$x = 0.10$	A-10	1100	97.8	1.33

3.2 High-temperature dielectric properties

The temperature-dependent dielectric constant and dielectric loss for $(1 - x)$ (BNT-BT)- x AN ceramics measured at 1 kHz, 10 kHz, 100 kHz, and 1 MHz are evaluated and shown in Fig. 3. The dielectric properties of pure BNT-BT ($x = 0$) were reported in our previous work [15]. Two distinct dielectric anomalies in dielectric curves can be determined for all compositions, corresponding to the shoulder temperature (T_s) and maximum temperature (T_m), respectively. At T_s , the strong frequency dispersion of both permittivity and dielectric loss can be found, as denoted in Fig. 3a by solid arrows. It is worth mentioning that the temperature corresponding to the dielectric loss peak was also considered to be the depolarization temperature in some literatures [19, 20]. Permittivity at T_s was around 3300 in the composition $x = 0.01$ at 1 kHz. The other characteristic temperature T_m was evolved from the Curie point, at which the dielectric peak was relatively flat and broad. Permittivity at T_m was around 4500 in

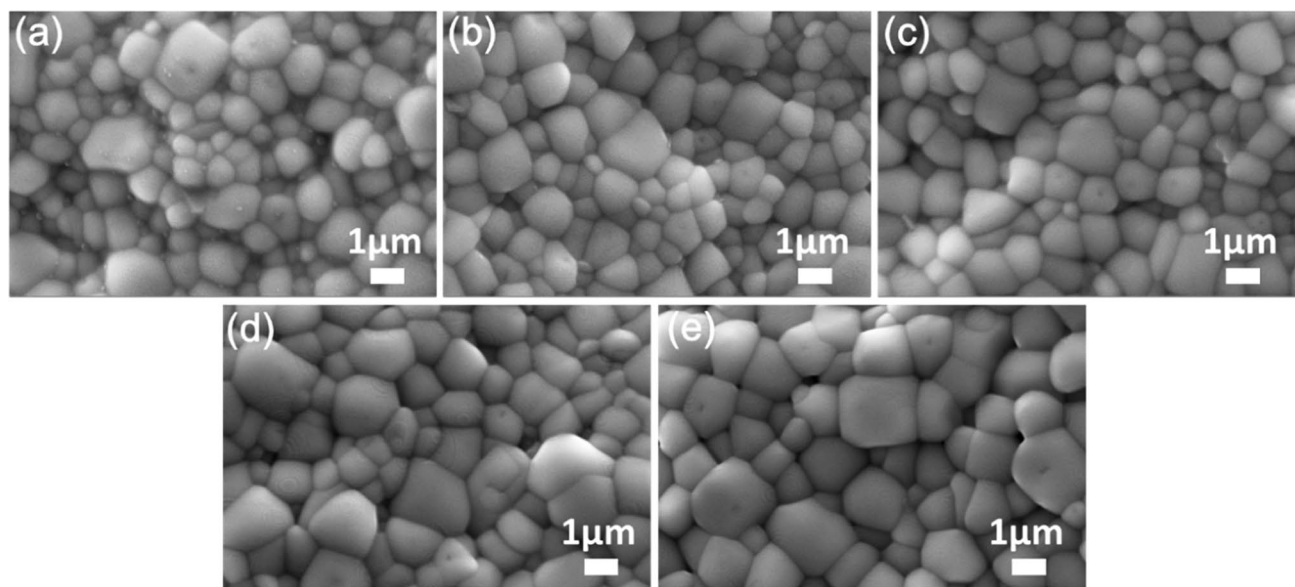


Fig. 2 Cross-section SEM images of $(1 - x)$ (BNT-BT)- x AN ceramics: **a** $x = 0.01$, **b** $x = 0.03$, **c** $x = 0.05$, **d** $x = 0.07$, and **e** $x = 0.10$

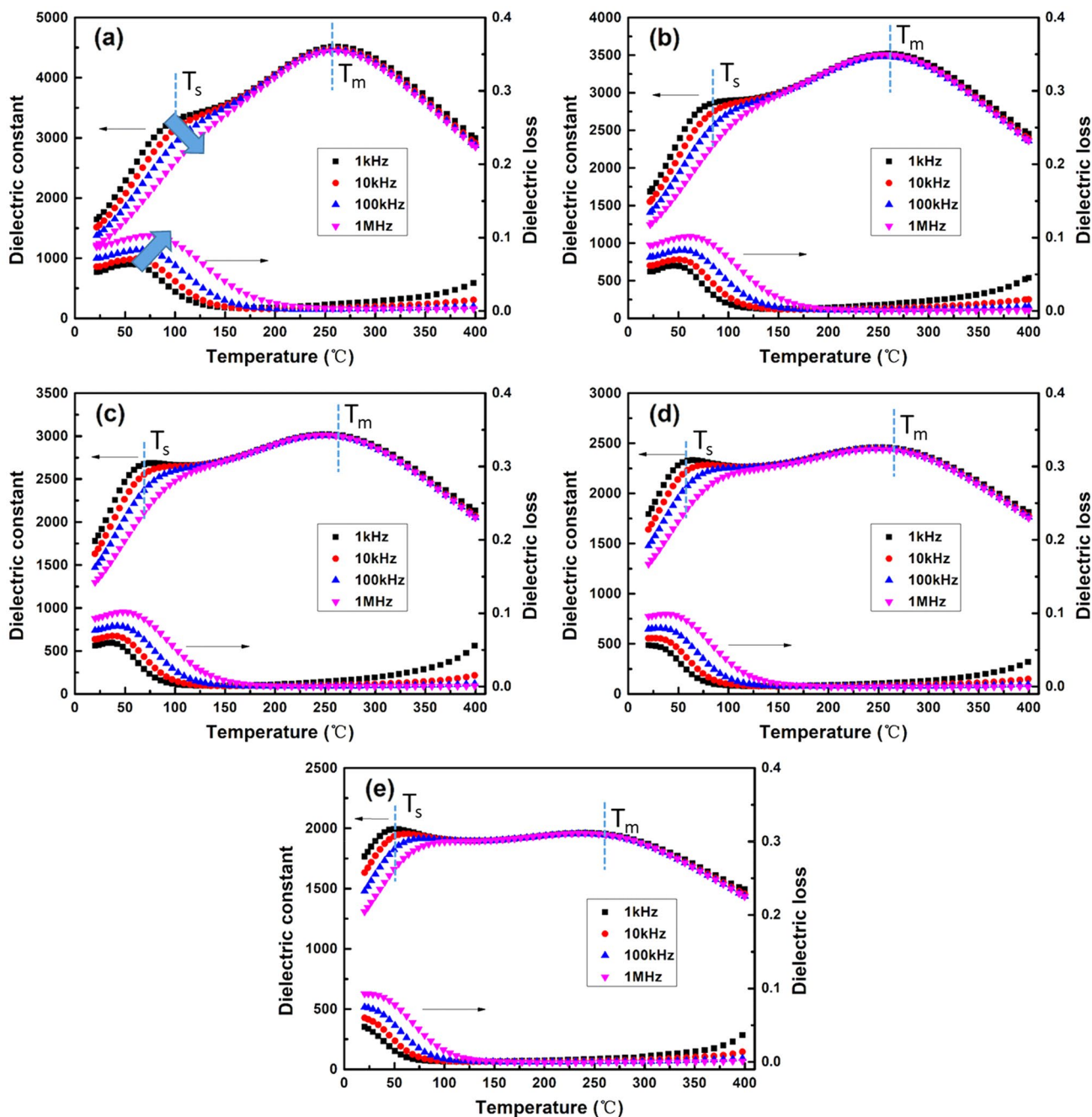


Fig. 3 Temperature-dependent dielectric constant and dielectric loss of $(1 - x)(\text{BNT-BT})\text{-}x\text{AN}$ ceramics: **a** $x=0.01$, **b** $x=0.03$, **c** $x=0.05$, **d** $x=0.07$, and **e** $x=0.10$

the composition $x=0.01$ at 1 kHz. It was clear that a large gap existed in the permittivity between T_s and T_m .

With increasing AN content, both the dielectric anomalies changed, as shown in Fig. 3b–e. T_s shifted to lower temperature ($97\text{ }^\circ\text{C} \rightarrow 81\text{ }^\circ\text{C} \rightarrow 64\text{ }^\circ\text{C} \rightarrow 54\text{ }^\circ\text{C} \rightarrow 45\text{ }^\circ\text{C}$ for composition $x=0.01 \rightarrow x=0.03 \rightarrow x=0.05 \rightarrow x=0.07 \rightarrow x=0.10$ at 1 kHz) and the permittivity at T_s slightly decreased ($3300 \rightarrow 2850 \rightarrow 2650 \rightarrow 2310 \rightarrow 1980$ for composition $x=0.01$

$\rightarrow x=0.03 \rightarrow x=0.05 \rightarrow x=0.07 \rightarrow x=0.10$ at 1 kHz). While at T_m , the dielectric peak was largely depressed. The permittivity at T_m slumped from 4500 in $x=0.01$ to 1950 in $x=0.10$ at 1 kHz. The variation of the permittivity gaps between T_s and T_m led to more flat permittivity curves. Similar dielectric behavior was also reported in BNT-BT-CaZrO₃ [21 and BNT-BT-K_{0.5}Na_{0.5}NbO₃ [22 ceramics. It was commonly considered that in BNT-based systems, the dielectric

anomaly at T_s resulted from the thermal evolution of rhombohedral R3c and tetragonal P4bm polar nano regions (PNRs), while the dielectric anomaly at T_m was attributed to R3c-P4bm transition and the thermal evolution of P4bm PNRs [23]. In this study, it was supposed that for the composition with a small amount of AN, polar rhombohedral PNRs with large quantity and dimension dominated. With the increase of AN content, the proportion of polar rhombohedral PNRs largely reduced, while weakly polar tetragonal PNRs dominated around T_m .

Favorable high-temperature stability of permittivity was obtained due to the depressed dielectric curves. Figure 4 illustrates the temperature coefficient of capacitance based on 150 °C ($TCC_{150\text{ }^\circ\text{C}}$) of $(1-x)$ (BNT-BT)- x AN ceramics at the frequency of 1 kHz. The dashed lines indicate the operational ranges within 15%. $TCC_{150\text{ }^\circ\text{C}}$ can be calculated according to the equation of $TCC_{150\text{ }^\circ\text{C}} = \Delta C/C_{150\text{ }^\circ\text{C}} = (C_T - C_{150\text{ }^\circ\text{C}})/C_{150\text{ }^\circ\text{C}}$. For composition $x=0.01$, the working temperature range satisfying $\Delta C/C_{150\text{ }^\circ\text{C}} \leq 15\%$ lay in the range 80–202 °C. With the increase of AN content, the temperature range was largely broadened. For $x=0.10$, the lower limit temperature dropped to 20 °C and the upper limit temperature rose up to 368 °C, demonstrating a 348

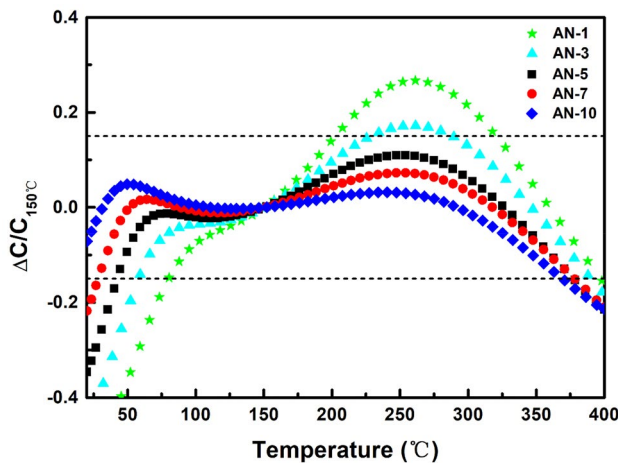


Fig. 4 $TCC_{150\text{ }^\circ\text{C}}$ of $(1-x)$ (BNT-BT)- x AN ($x=0.05\text{--}0.10$) ceramics at the frequency of 1 kHz

Table 2 Dielectric properties of $(1-x)$ (BNT-BT)- x AN ceramics

Sample	ϵ_r (25 °C, 1 kHz)	$\tan\delta$ (25 °C, 1 kHz)	ϵ_r (150 °C, 1 kHz)	$\tan\delta$ (150 °C, 1 kHz)	$\Delta C/C_{150\text{ }^\circ\text{C}} \leq 15\%$ range (°C)
A-1	1702	0.054	3564	0.005	80–202
A-3	1744	0.054	3003	0.003	59–228
A-5	1889	0.057	2722	0.001	43–377
A-7	1883	0.056	2293	0.001	29–378
A-10	1826	0.044	1901	0.001	20–368

ultra-wide range. Table 2 lists the dielectric constant and dielectric loss at 25 °C and 150 °C of all the samples.

It was reported that in BNT-BT-NaTaO₃ system, the working temperature range satisfying $\Delta C/C_{150\text{ }^\circ\text{C}} \leq 15\%$ was around 260 °C with room temperature permittivity of 1472–1785 [24]. In BNT-BT-Na_{1-3y}Bi_yNbO₃ system, the operation range spanned over 327 °C for $\pm 15\%$ tolerance with $\epsilon_r 25\text{ }^\circ\text{C} = 1610\text{--}1750$ [16]. Compared to the reported BNT-based ceramics, 0.90(BNT-BT)-0.10AN presented higher permittivity and superior high-temperature stability. The evolution of T_s and T_m and the corresponding reduction in permittivity were responsible for the expansion of working temperature range.

3.3 Electrical insulation

The electrical insulation property of capacitors is also a parameter that should not be ignored. For capacitors applied at high temperature, we should not only pay attention to the insulation property at room temperature, but also its variation with temperature. RC constant (or “time constant”) is often used to characterize the electrical insulation property of capacitors or dielectric materials. It measures the ability to charge retention. In a discharging process of capacitors, the charge at time t ($Q(t)$) can be expressed as follows: $Q(t) = Q_0 \cdot \exp(-\frac{t}{\tau})$ [22]. Q_0 is the initial charge, τ is the time constant, and $\tau = RC$. When $t = \tau = RC$, $Q(t) = Q_0 \cdot \exp(-1)$, which means that the charge drops to e^{-1} ($\approx 37\%$) of the initial value. Hence, the larger the RC constant, the longer the dielectric can hold the charge above 37%.

Figure 5 shows the RC time constant as a function of temperature plot of 0.90(BNT-BT)-0.10AN ceramic sample. The RC constant was above 12 s upto 240 °C. With further rise of temperature, it decreased to 0.6 s at ~ 300 °C. This value is comparable to other reported ceramic systems such as BNT-BT-0.2CZ [21], BiScO₃-PbTiO₃ [25], and BNT-BT-K_{0.5}Na_{0.5}NbO₃ [22, 26]. However, as a potential future material in high-temperature capacitors, the insulation resistivity of 0.90(BNT-BT)-0.10AN still needs further improvement.

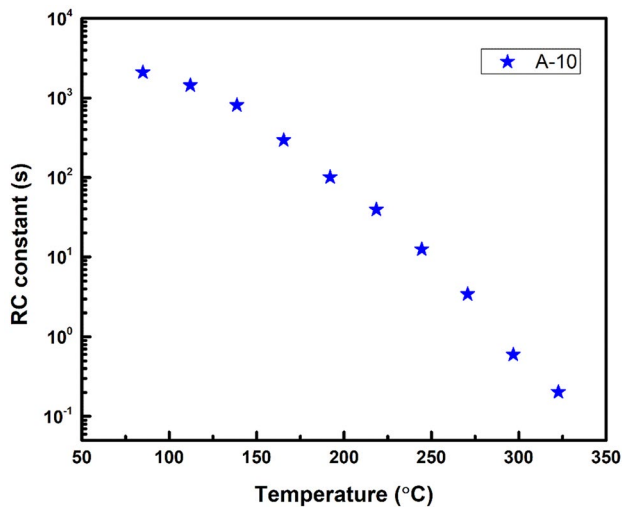


Fig. 5 RC constant as a function of temperature plot of 0.90(BNT-BT)-0.10AN ceramic sample

3.4 Energy-storage properties

Figure 6 shows the P–E and I–E loops of $(1-x)$ (BNT-BT)- x AN ceramics at 7 kV/mm. When small amount of AN was added (sample $x = 0.01$), slightly pinched P–E hysteresis loop can be observed, as shown in Fig. 6a. The maximum polarization P_m reached $47\mu\text{C}/\text{cm}^2$ and the remanent polarization P_r remained $17\mu\text{C}/\text{cm}^2$. The corresponding I–E loop was demonstrated in Fig. 6b. Four current peaks were obvious in the loop, which were denoted as “I”, “II”, “III”, and “IV”. Peak “I” represented a transition from relaxor state to ferroelectric state at an electric field of ~ 3.8 kV/mm. When unloading the electric field, most part of the effect can be recovered. Only by reversing the electric field to -3.8 kV/mm, all the effect produced in the first quadrant can be completely recovered. These two processes corresponded to peak “II” and “III”, respectively. The current peak “IV” represented the opposite process.

With the increase of AN content (samples $x=0.03$ – 0.07), P–E hysteresis loops still exhibited pinched shape and became slimmer. P_m decreased from $47\mu\text{C}/\text{cm}^2$ in $x=0.01$ to $26\mu\text{C}/\text{cm}^2$ in $x=0.07$ and P_r declined from $17\mu\text{C}/\text{cm}^2$ in $x=0.01$ to $1.3\mu\text{C}/\text{cm}^2$ in $x=0.07$, as shown in Fig. 7a. In I–E loops, four current peaks still existed. But they became obscure and shifted to higher electric field gradually. Further increase of AN (sample $x=0.10$) led to almost linear P–E hysteresis loop with P_r close to zero, as shown in Fig. 6i. I–E loop exhibited rectangle shape with no obvious current peak.

It is obvious that the ferroelectric properties of BNT-BT system had experienced a great change by the introduction of AN. Similar phenomenon has been reported in other BNT-based ternary solid solution [27, 28]. It is commonly considered that BNT-BT ceramics are relaxor ferroelectrics rather

than anti-ferroelectric materials. In this work, the composition with $x=0.01$ is supposed to be a non-ergodic relaxor, in which static polar nanodomains instead of ferroelectric domain dominate. Under electric field, the static polar nanodomains are poled and aligned, resulting in P_r in P–E loop. With the increase of AN content ($x=0.03$ – 0.07), ceramics turn into ergodic relaxor. In these samples, polar regions become smaller in size, being called “dynamic polar nanoregions” (PNRs). Thus, not only the electric field-induced polarization decreases, but also they would dribble away when the electric field is removed, leading to reduced P_m and P_r . Composition with higher AN content ($x=0.10$) exhibits paraelectric state at room temperature, owing to the increment of charge disorder [29].

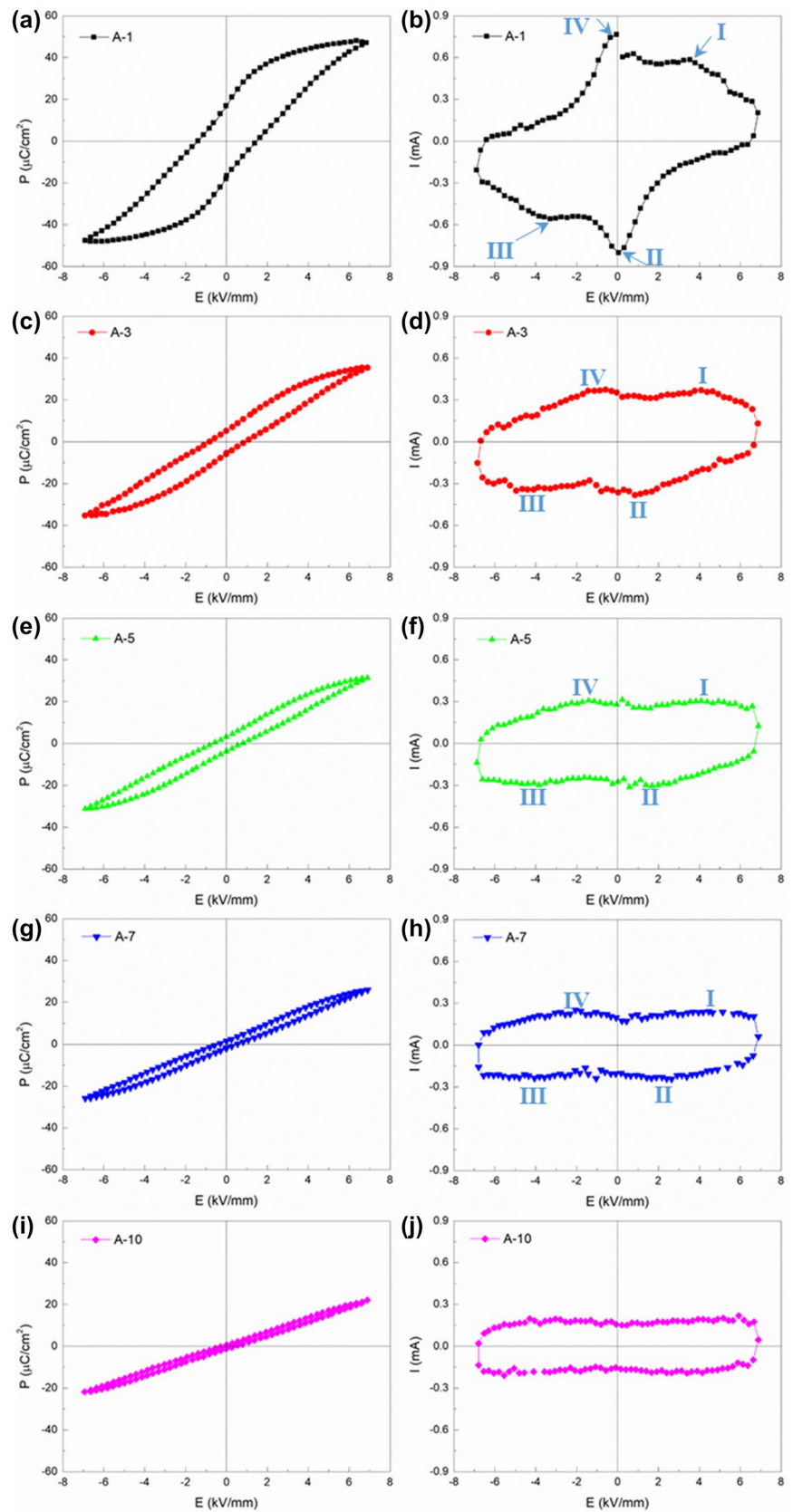
According to the P–E loops under 7 kV/mm, the energy-storage parameters of $(1-x)$ (BNT-BT)- x AN ceramics can be calculated by the formulas $W = \int_0^E EdP$ [30] and $\eta = W/W'$, in which W , W' , and η refer to discharge energy-storage density, charge energy-storage density, and energy-storage efficiency, respectively. As shown in Fig. 7b, with the addition of AN from $x=0.01$ to $x=0.05$, the energy-storage density increased from 0.51 to 0.81 J/cm³ on account of the sharp decline of P_r . Further increase of AN reduced the value to 0.68 J/cm³ in $x=0.10$, which was resulted from the decline of P_m . On the other hand, due to the continuous degradation of ferroelectric behavior and slimming of P–E loop, the energy-storage efficiency kept rising from 28% in $x=0.01$ to 81% in $x=0.10$.

Since most electronic devices will be used at high-voltage environment, the critical electric field (the maximum electric field before breakdown) and energy-storage properties under which were also be tested. As shown in Fig. 8, P–E loops of $(1-x)$ (BNT-BT)- x AN ceramic samples under critical electric field were still pinched and became more slanted with increasing AN. The critical electric fields of all the compositions were higher than 9.4 kV/mm (sample thickness ~ 0.3 mm). It was comparable to ferroelectric ceramics like BaTiO₃-based systems [31], but a certain gap still existed compared to traditional paraelectric dielectrics like SrTiO₃-based systems [32, 33]. Despite that, the energy-storage density under critical electric field reached 1.26 J/cm³ in the composition $x=0.05$ due to the large polarization P_m . The energy-storage efficiency increased from 33% in $x=0.01$ to 78% in $x=0.10$. Taking an overall consideration of these two parameters, the optimum energy-storage properties were obtained in $x=0.10$ with $W_{\max} = 1.07$ J/cm³ and $\eta_{\max} = 78\%$ under 10.4 kV/mm.

4 Conclusions

The structure, dielectric, and energy-storage properties of $(1-x)$ (BNT-BT)- x AN ceramics prepared by solid-state reaction method were investigated. XRD analysis indicated

Fig. 6 P–E and I–E loops of $(1-x)(\text{BNT-BT})$ - $x\text{AN}$ ceramics at 7 kV/mm



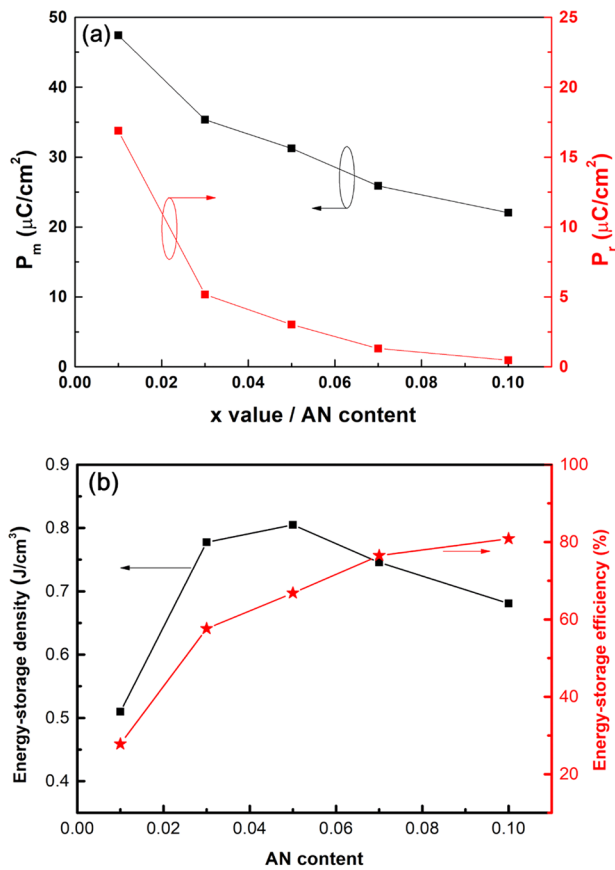


Fig. 7 P_m , P_r , and energy-storage density and efficiency of $(1-x)$ (BNT-BT)- x AN ceramics at 7 kV/mm

that all the samples exhibited pure perovskite phase with no secondary impurity. Rhombohedral and tetragonal phase coexisted in $x=0.01$. With increasing AN content, it became pseudo cubic structure. Attractive dielectric properties were obtained in the sample $x=0.10$ at less than 15% variation of relative permittivity of about 1901 between 20 and 368 °C. The RC constant was above 12 s up to 240 °C. Taking an overall consideration of energy-storage density and efficiency, the optimum energy-storage properties were obtained in $x=0.10$ with $W_{\max}=1.07 \text{ J}/\text{cm}^3$ and $\eta_{\max}=78\%$ under 10.4 kV/mm.

Acknowledgements This work was supported by National Natural Science Foundation of China (No. 51372191), Start-up Grant of Chengdu University of Technology (Grant No. 10900-KYQD-06848), and Natural Science Youth Foundation of Anhui Province (Grant No. 1808085QE153).

References

1. R.R. Grzybowski, B. Gingrich, High temperature silicon integrated circuits and passive components for commercial and

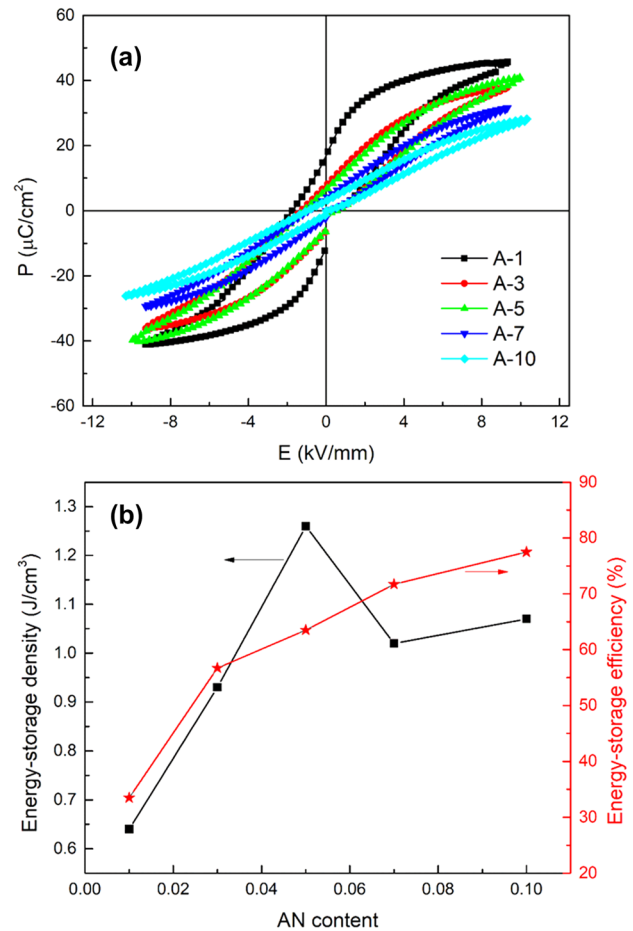


Fig. 8 a P-E loops and b energy-storage properties of $(1-x)$ (BNT-BT)- x AN ceramics under critical electric field

2. X. Hao, A review on the dielectric materials for high energy-storage application. *J. Adv. Dielectr.* **03**(01), 1330001 (2013)
3. T. Wang, L. Jin, C. Li et al., Relaxor ferroelectric $\text{BaTiO}_3\text{-Bi}(\text{Mg}_{2/3}\text{Nb}_{1/3})\text{O}_3$ ceramics for energy storage application. *J. Am. Ceram. Soc.* **98**(2), 559–566 (2015)
4. H. Lee, J.R. Kim, M.J. Lanagan et al., High-energy density dielectrics and capacitors for elevated temperatures: $\text{Ca}(\text{Zr,Ti})\text{O}_3$. *J. Am. Ceram. Soc.* **96**(4), 1209–1213 (2013)
5. C.A. Randall, H. Ogihara, J.-R. Kim et al in High temperature and high energy density dielectric materials. Pulsed Power Conference. PPC '09. IEEE (2009)
6. C. Ma, X. Tan, E. Dul'kin et al., Domain structure-dielectric property relationship in lead-free $(1-x)(\text{Bi}_{1/2}\text{Na}_{1/2})\text{TiO}_3\text{-xBaTiO}_3$ ceramics. *J. Appl. Phys.* **108**(10), 104105 (2010)
7. Y. Yuan, E.Z. Li, B. Li et al., Effects of Ca and Mn additions on the microstructure and dielectric properties of $(\text{Bi}_{0.5}\text{Na}_{0.5})\text{TiO}_3$ ceramics. *J. Electron. Mater.* **40**(11), 2234–2239 (2011)
8. F. Gao, X. Dong, C. Mao et al., Energy-storage properties of $0.89\text{Bi}_{0.5}\text{Na}_{0.5}\text{TiO}_3\text{-}0.06\text{BaTiO}_3\text{-}0.05\text{K}_{0.5}\text{Na}_{0.5}\text{NbO}_3$ lead-free anti-ferroelectric ceramics. *J. Am. Ceram. Soc.* **94**(12), 4382–4386 (2011)

9. Y. Yuan, X.H. Zhou, C.J. Zhao et al., High-temperature capacitor based on Ca-doped $\text{Bi}_{0.5}\text{Na}_{0.5}\text{TiO}_3\text{-BaTiO}_3$ ceramics. *J. Electron. Mater.* **39**(11), 2471–2475 (2010)
10. G. Viola, H. Ning, M.J. Reece et al., Reversibility in electric field-induced transition and energy storage properties of bismuth-based perovskite ceramics. *J. Phys. D* **45**(35), 355302 (2012)
11. B.S. Utami, C.-N. Chen, C.-C. Chou et al., Temperature dependent phase transition of $(\text{Bi}_{0.5}\text{Na}_{0.5})_{1-x}\text{Ba}_x\text{TiO}_3$ lead-free piezoelectric. *Ceram. Int.* **39**, S175–S179 (2013)
12. T. Oh, M.-H. Kim, Phase relation and dielectric properties in $(\text{Bi}_{1/2}\text{Na}_{1/2})_{1-x}\text{Ba}_x\text{TiO}_3$ lead-free ceramics. *Mater. Sci. Eng. B* **132**(3), 239–246 (2006)
13. Y.-T. Shih, J.-H. Jean, S.-C. Lin, Failure mechanism of a low-temperature-cofired ceramic capacitor with an inner Ag electrode. *J. Am. Ceram. Soc.* **93**(10), 3278–3283 (2010)
14. W.H. Lu, Y.C. Lee, P.R. Tsai, Effect of sintering parameters on silver diffusion of $(\text{Zn,Mg})\text{TiO}_3$ based multilayer ceramic capacitors. *Adv. Appl. Ceram.* **110**(2), 99–107 (2011)
15. Q. Xu, T. Li, H. Hao et al., Enhanced energy storage properties of NaNbO_3 modified $\text{Bi}_{0.5}\text{Na}_{0.5}\text{TiO}_3$ based ceramics. *J. Eur. Ceram. Soc.* **35**(2), 545–553 (2015)
16. Q. Xu, H. Liu, J. Xie et al., High-temperature dielectrics in BNT-BT based solid solution. *IEEE Trans. Ultrason.* **63**, 1656 (2016)
17. Q. Xu, H. Liu, Z. Song et al., A new energy-storage ceramic system based on $\text{Bi}_{0.5}\text{Na}_{0.5}\text{TiO}_3$ ternary solid solution. *J. Mater. Sci. Mater. Electron.* **27**(1), 322–329 (2016)
18. Q. Xu, M. Chen, W. Chen et al., Effect of CoO additive on structure and electrical properties of $(\text{Na}_{0.5}\text{Bi}_{0.5})_{0.93}\text{Ba}_{0.07}\text{TiO}_3$ ceramics prepared by the citrate method. *Acta Mater.* **56**(3), 642–650 (2008)
19. D. Schütz, M. Deluca, W. Krauss et al., Lone-pair-induced covalency as the cause of temperature- and field-induced instabilities in bismuth sodium titanate. *Adv. Funct. Mater.* **22**(11), 2285–2294 (2012)
20. J. Wang, Q. Li, Y. Ma et al., The electrocaloric effect and thermal stability of $0.94(\text{Bi}_{0.5}\text{Na}_{0.5})\text{TiO}_3\text{-}0.06\text{BaTiO}_3$ modified by WO_3 . *Appl. Phys. A*, 2016, 122(5):517
21. M. Acosta, J. Zang, W. Jo et al., High-temperature dielectrics in CaZrO_3 -modified $\text{Bi}_{1/2}\text{Na}_{1/2}\text{TiO}_3$ -based lead-free ceramics. *J. Eur. Ceram. Soc.* **32**(16), 4327–4334 (2012)
22. R. Dittmer, W. Jo, D. Damjanovic et al., Lead-free high-temperature dielectrics with wide operational range. *J. Appl. Phys.* **109**(3), 034107 (2011)
23. W. Jo, S. Schaab, E. Sapper et al., On the phase identity and its thermal evolution of lead free $(\text{Bi}_{1/2}\text{Na}_{1/2})\text{TiO}_3\text{-}6\text{ mol\% BaTiO}_3$. *J. Appl. Phys.* **110**(7), 074106 (2011)
24. Q. Xu, H. Liu, L. Zhang et al., Structure and electrical properties of lead-free $\text{Bi}_{0.5}\text{Na}_{0.5}\text{TiO}_3$ -based ceramics for energy-storage applications. *RSC Adv.* **6**(64), 59280–59291 (2016)
25. S. Zhang, E.F. Alberta, R.E. Eitel et al., Elastic, piezoelectric, and dielectric characterization of modified $\text{BiScO}_3\text{-PbTiO}_3$ ceramics. *IEEE Trans. Ultrason.* **52**(11), 2131–2139 (2005)
26. C. Groh, K. Kobayashi, H. Shimizu et al., High-temperature multilayer ceramic capacitors based on $100 - x(94\text{Bi}_{1/2}\text{Na}_{1/2}\text{TiO}_3\text{-}6\text{BaTiO}_3)\text{-}x\text{K}_{0.5}\text{Na}_{0.5}\text{NbO}_3$. *J. Am. Ceram. Soc.* **99**(6), 2040–2047 (2016)
27. J. Hao, Z. Xu, R. Chu et al., Field-induced large strain in lead-free $(\text{Bi}_{0.5}\text{Na}_{0.5})_{1-x}\text{Ba}_x\text{Ti}_{0.98}(\text{Fe}_{0.5}\text{Ta}_{0.5})_{0.02}\text{O}_3$ piezoelectric ceramics. *J. Alloys Compd.* **677**, 96–104 (2016)
28. X.L. Zhao, W.Z. Yang, X.Q. Liu et al., Dielectric and ferroelectric characteristics of $[(\text{Bi}_{0.5}\text{Na}_{0.5})_{0.94}\text{Ba}_{0.06}]_{1-x}\text{Sr}_x\text{TiO}_3$ ceramics[J]. *J. Mater. Sci.* **25**(3), 1517–1526 (2014)
29. D. Gobeljic, R. Dittmer, J. Rödel et al., Macroscopic and nanoscopic polarization relaxation kinetics in lead-free relaxors $\text{Bi}_{1/2}\text{Na}_{1/2}\text{TiO}_3\text{-Bi}_{1/2}\text{K}_{1/2}\text{TiO}_3\text{-BiZn}_{1/2}\text{Ti}_{1/2}\text{O}_3$. *J. Am. Ceram. Soc.* **97**(12), 3904–3912 (2014)
30. N.H. Fletcher, A.D. Hilton, B.W. Ricketts, Optimization of energy storage density in ceramic capacitors. *J. Phys. D* **29**(1), 253–258 (1996)
31. W. Deng, J.F. Nie, X. Xiao et al., Effect of $\text{Bi}_2\text{O}_3\text{-B}_2\text{O}_3\text{-CuO}$ additives on dielectric properties and energy storage of BaTiO_3 ceramics. *Key Eng. Mater.* **512–515**, 1146–1149 (2012)
32. G. Zhao, Y. Li, H. Liu et al., Effect of SiO_2 additives on the microstructure and energy storage density of SrTiO_3 ceramics. *J. Ceram. Process. Res.* **13**(3), 310–314 (2012)
33. L. Li, X. Yu, H. Cai et al., Preparation and dielectric properties of $\text{BaCu}(\text{B}_2\text{O}_5)$ -doped SrTiO_3 -based ceramics for energy storage. *Mater. Sci. Eng. B* **178**(20), 1509–1514 (2013)

Publisher's Note Springer Nature remains neutral with regard to jurisdictional claims in published maps and institutional affiliations.